NUMERICAL CALIBRATION OF BOND LAWS FOR GFRP BARS EMBEDDED IN STEEL FIBRE-REINFORCED SELF-COMPACTING CONCRETE

M. Pepe [1], H. Mazaheripour[2], J. Barros[2], J. Sena-Cruz[2], E. Martinelli[1]

[1] Dep. Civil Eng., University of Salerno, Fisciano, Italy

[2] ISISE, Dep. Civil Eng., Minho University, Guimarães, Portugal

Marco Pepe, Ph.D. Candidate,

e.mail: mapepe@unisa.it; Dept. of Civil Engineering, University of Salerno, IT

Hadi Mazaheripour, Ph.D. Candidate,

e.mail: hmp@civil.uminho.pt; ISISE, Dept. of Civil Eng., Minho University, Guimarães, PT

Joaquim A.O. Barros, Full Professor of Structural Engineering,

e.mail: barros@civil.uminho.pt; ISISE, Dept. Civil Eng., Minho University, Guimarães, PT

José Sena-Cruz, Associate Professor of Structural Engineering,

e.mail: jsena@civil.uminho.pt; ISISE, Dept. Civil Eng., Minho University, Guimarães, PT

Enzo Martinelli, Assistant Professor of Structural Engineering,

Dept. of Civil Eng., University of Salerno, via Ponte don Melillo, 84084, Fisciano SA, IT

e.mail: e.martinelli@unisa.it; Dept. of Civil Engineering, University of Salerno, IT

ABSTRACT

An experimental program was carried out at the Laboratory of Structural Division of the Civil Engineering Department of the University of Minho (LEST-UM) to investigate the bond behaviour of glass fibre reinforced polymer (GFRP) bars embedded in steel fibre reinforced self-compacting concrete (SFRSCC) for the development of an innovative structural system. Thirty-six pull-out-bending tests were executed to assess the influence of the bond length, concrete cover, bar diameter and surface treatment on the bond of GFRP bars embedded in SFRSCC. This paper reports the results of a numerical study aiming to identify an accurate GFRP–SFRSCC bond-slip law. Thus, the above mentioned pullout bending tests were simulated by using a nonlinear finite element (FE) constitutive model available in FEMIX, a FEM based computer program. The bond-slip relationship adopted for modelling the FE interface that simulates the interaction between bar and concrete is the key nonlinear aspect considered in the FE analyses, but the nonlinear behaviour of SFRSCC due to crack initiation and propagation was also simulated. The evaluation of the values of the relevant parameters defining such a bond-slip relationship was executed by fitting the force versus loaded end slip responses recorded in the experimental tests. Finally, correlations are proposed between the parameters identifying the bond-slip relationship and the relevant geometric and mechanical properties of the tested specimens.

KEYWORDS: A. Glass fibres; B. Fibre/matrix bond; C. Finite Element Analysis (FEA); D. Mechanical testing

1 INTRODUCTION

Although reinforced concrete (RC) structures are rather common in developed countries, several critical issues emerged recently about their durability and maintenance costs that can be assessed through life cycle analyses [1]. As a matter of fact, material degradation is not only detrimental under the aesthetic standpoint, but can even jeopardise the safety level of structures [2]. Moreover, due to both historical and economic reasons (i.e. urgency of post-war reconstruction, exasperated structural lightness, low accuracy on design detailing, etc.) concrete structures were not generally designed with the due attention to durability-related issues. Degradation phenomena in concrete structures are often related to corrosion of steel reinforcement [3], which can occur after carbonation [4] of concrete cortical layers in members exposed to water, humidity or other severe environmental conditions [5].

Durability issues related to the possible oxidation of steel reinforcement in concrete structures have recently brought the attention of civil engineers towards alternative materials for reinforcing systems [6]. Fibre Reinforced Polymers (FRP), which were initially developed and employed in the aerospace, aeronautics, naval and automotive industries, generally exhibit high mechanical and durability performance. Thus, the research activities in this field are supporting the publication of design guidelines on the use of FRP as internal reinforcement of cement-based composite members [7][8][9] and, then, FRP bars are becoming more common in the construction sector [10].

In fact, reinforcing bars made of Glass Fibre Reinforced Polymers (GFRP) are currently employed as a feasible alternative to conventional steel bars for RC structures [11]. However, the relatively low modulus of elasticity of GFRP bars, their linear stress-strain behaviour up to failure, their brittle behaviour, creep rupture and the lack of a complete understanding of their bond to cement-based matrices are key aspects to be correctly addressed for a sound and reliable design of concrete structures reinforced with GFRP bars. Special care should be given to the relatively low elasticity modulus and bond properties due to its relevant influence on the deflection and cracking at the Serviceability Limit States (SLS) of GFRP reinforced concrete structural elements [12] [13].

Bond between steel bars and concrete has been widely studied in the last decades and several codes and guidelines have been issued for providing practitioners with sound design rules [15].

The interest for describing the bond behaviour of FRP bars (either made of carbon, aramid, basalt or glass fibres) is more recent, as the use of FRP materials emerged in the last decade as a feasible and often effective solution for reinforcing concrete structures [16][17]. However, the notable interest of the scientific community on the use of FRP systems for the strengthening and reinforcement of concrete structures during the last 20 years has generated plenty of data in this field, in consequence of the experimental, numerical and analytical research. For instance, Daniali [18] examined the behaviour of glass fibre deformed bars, Tepfers et al. [19] performed pull-out tests on concrete reinforced with carbon fibre and aramid fibre strands, and Malvar [20][21] analysed the influence of surface treatment on bond behaviour. Moreover, several proposals for theoretical models addressing the issue of bond for FRP bars in concrete are currently available in the scientific literature (e.g., Eligehausen et al. [22], Cosenza et al. [23], Rossetti et al. [24], Tepfers and De Lorenzis [25], Malvar [26], Sena and Barros [27], Bianco et al. [28]).

As a matter of fact, the bond interaction of FRP bars is more complex than generally accepted for steel bars in concrete. Such a higher complexity derives from the wider range of variation of the geometric and mechanical properties of FRP bars with respect to steel ones. For instance, various surface treatments (i.e., smooth, sanded coated, braided deformed, spiral deformed, etc.) are currently available for FRP bars and play a significant role on the bond performance and on the derived consequences. Thus, many different key parameters influence the bond between FRP and concrete: in principle, they could include surface conditions, modulus of elasticity, shear and axial stiffness, bar diameter, bond length, etc. [29]. Bond between FRP bars and concrete is also controlled by other factors, including chemical bond, friction due to surface roughness of the FRP bars, mechanical interlock between FRP bars and concrete, confinement applied to the FRP bars due to concrete shrinkage or external loads, and swelling of FRP bars due to temperature variation and moisture absorption [30]. The chemical bond would be the primary resisting mechanism in the pull-out process of bars from concrete; thereafter, mechanical interlock and friction could be the second and third reinforcing mechanisms, respectively.

The present study is part of a research project aiming to develop high performance fibre reinforced concrete (HPFRC) flexurally reinforced by hybrid pre-stressed GFRP/Steel bars. The objective of using this hybrid system is to propose a reinforcing solution based on employing both steel and GFRP reinforcing pre-stressed bars, the former being protected by a concrete cover (60 mm or even more) that is thicker than the cover of the GFRP bars, which are mounted as close as possible to the outer surface of the concrete member under consideration. Additionally, within the framework of the ongoing research project, a steel fibre reinforced self-compacting concrete (SFRSCC) with relatively high amount of steel fibres (more than 60 kg/m^3) is considered with the aim of eliminating the steel stirrups generally needed as a shear reinforcement of concrete beams. SFRSCC and a flexural reinforcement system composed of hybrid steel/GFRP pre-stressed bars constitute the main innovative aspects of a new generation of high durable corrosion-free precast beams. To assess the possibility of using this reinforcement solution, the study was firstly based on an extensive experimental program aiming to investigate the bond behaviour between GFRP bars and SFRSCC, by means of pull-out bending tests carried out adopting an experimental setup similar to one recommended by RILEM for steel bars [31].

Within this general framework, the present study proposes the calibration of bond-slip relationships [14] that characterise the behaviour of GFRP bars embedded in SFRSCC. Particularly, this paper reports the key achievements of a numerical investigation carried out to identify the bond-slip relationships resulting from a back-analysis of the results of thirty-six pull-out bending tests performed on SFRSCC specimens reinforced with GFRP bars [31]. The effect of several properties (namely, bond length, bar diameter, concrete cover, and surface treatment of bars) was investigated, as they are supposed to play a relevant role in influencing the interaction between concrete and reinforcement. Section 2 of the present paper outlines the key mechanical properties of materials employed in the tested specimens and summarises the results of those thirty-six pull-out bending tests presented in [31]. Then, Section 3 describes the numerical simulations of such tests carried out by using the FEMIX software [32]. Particularly, the geometry, boundary conditions and constitutive laws of materials adopted in the FEM model are presented. Furthermore, Section 4 reports

and analyses the obtained results and, finally, Section 5 proposes possible correlations between the parameters identifying the bond-slip relationship and the relevant geometric and mechanical properties of the tested specimens.

2 OUTLINE OF THE EXPERIMENTAL RESULTS

Thirty-six pull-out-bending tests (based on the RILEM standard [33]) were carried out at the Laboratory of Structural Division of the Civil Engineering Department of the University of Minho (LEST-UM) with the aim of investigating the influence of the following characteristics on the bond behaviour between GFRP bars and SFRSCC:

- bar surface treatment: sand-coated; ribbed;
- bar diameter (Φ):8 mm; 12 mm;
- concrete cover thickness: 15 mm; 30 mm;
- bond length, defined in terms of a multiple of the nominal bar diameter: 10Φ; 20Φ.

Table 1 and Table 2 show the main properties that characterise the mechanical behaviour of both SFRSCC and GFRP bars. The full characterisation of the post-cracking flexural behaviour of SFRSCC and the tensile behaviour of GFRP bars are detailed in another paper [31]. Moreover, Table 3 summarises the pull-out-bending test program carried out.

For this experimental program, prismatic concrete specimens (820×200×150 mm^3) were used with a reinforcing GFRP bar embedded inside, near to the bottom (tensile) surface of concrete blocks, with cover thickness values indicated in Table 3. Figure 2 shows the schematic view of the pull-out-bending test setup, consisting of two concrete blocks (A and B). A longer bond length (335 mm) was always assumed for the bar embedded within the block B, as debonding failure is aimed to occur in block A, where a much shorter bond length (ranging between five and twenty times the bar diameter) was taken.

Each test was monitored by means of several measurement instruments (Figure 2). A strain gauge was glued on the GFRP bar surface at the symmetry axis of the specimen to measure the axial strain developed in bar and determine the pull-out force at the loaded end by multiplying such a strain by the GFRP elasticity modulus and bar cross sectional area. Four different transducers were applied, the LVDT 1 and LVDT 2 for measuring the loaded and the free end slip, respectively, whereas LVDT 3 and LVDT 4 were installed near the symmetry axis to estimate the variation of the internal arm (distance between the contact point of the

steel hinge and the GFRP bar for an indirect assessment of the force applied to the GFRP bar). Furthermore, three load cells, C1, C2 and C3 were installed in order to be possible the determination of all the applied loads and reactions.

The relationships between the pull-out force F applied to the GFRP bar and the corresponding values of loaded end slip (s_l, by using the records in LVDT1 and subtracting the GFRP elastic deformation between the section of the GFRP bar where the LVTD1 is mounted and the loaded end section, which is 50 mm apart, Figure 2) and free end slip (s_f, by using the records in LVDT2) are the direct results obtained from these pull-out-bending tests. The numerical simulations performed in the following sections aim to determine the local-bond slip relationship by fitting the F-s responses obtained experimentally.

3 DEFINITION OF THE FE MODEL

The experimental tests introduced in Section 2 were simulated by using Finite Element (FE) models available in FEMIX, a FEM-based computer program [32].

The following subsections report relevant information about the key aspects of the adopted models in terms of geometry, boundary and loading conditions, and constitutive laws for the materials and GFRP-SFRSCC interface.

3.1 Geometry and boundary conditions

Figure 3 shows the FE mesh adopted in the simulations: only one block (actually the one with the shorter and variable bond length) is considered in the FE model, as a result of the assumed structural symmetry for the test setup.

Eight-node Plane Stress finite elements were employed for representing the concrete block, with a Gauss-Legendre integration scheme of 2×2, while 2-nodes Truss 2D elements were adopted to simulate the GFRP bars. Moreover, 4-nodes 2D Interface FE were introduced to connect the corresponding nodes of concrete and bar throughout the actual bond length that is one of the variables under consideration in this study on GFRP-SFRSCC interaction. A Gauss-Lobatto integration scheme was assumed for the aforementioned interface elements by considering 2 integration points.

The FE mesh shown in Figure 3 was the result of a sensitivity analysis about the influence of the mesh refinement on the results, and it was verified that a further refinement did not contribute significantly for the accuracy of the numerical simulations. The sensitivity analysis was performed by refining the mesh under linear elastic behaviour only to reach the stabilized results with a prescribed accuracy. The support and load conditions are also represented in Figure 3.

3.2 Constitutive laws of materials

3.2.1 Steel fibre-reinforced self-compacting concrete

The mechanical behaviour of SFRSCC employed to test the specimens under consideration was modelled within the framework of continuum and nonlinear fracture mechanics, by considering a stress-strain constitutive matrix that considers the influence of fibre reinforcement just after crack initiation, through a multidirectional smeared crack model described in detail elsewhere [34]. Fine and coarse river sand and crushed granite aggregates with maximum size of 12 mm were used, and 60 kg of hooked ends steel fibres per m^3 of concrete, with a length (L_f) of 33 mm, a diameter (d_f) of 0.55 mm, and an aspect ratio (L_f/d_f) of 60 were adopted to produce a SFRSCC that at 28 days had an average compressive strength of 63.7 MPa, measured through testing cylinder specimens with 300 mm of height and 150 mm of diameter. The same tests led to obtain an average Young's modulus of 30.4 GPa.

In the constitutive model adopted to simulate the behaviour of SFRSCC assumes linear and elastic behaviour if it is uncracked, or with cracks completely closed. This approach is deemed credible, as for this relatively small percentage of fibres the stress-strain relationship is not affected by the fibres, at least in the branch between strain at crack initiation and the strain at peak compressive strength. Furthermore, the maximum compressive stress obtained in the analysis is relatively small compared to the compressive strength of this material. Therefore, the model adopted to simulate the behaviour of SFRSCC is focalized on the nonlinearities resulting from the crack initiation and propagation.

Several three-point notched beam bending tests were carried out according to the CEB-FIP Model Code 2010 [35] for characterizing the post-cracking behaviour of SFRSCC. The applied force (F) *versus* both the crack mouth opening displacement (CMOD) and mid-span deflection (δ) were obtained for the five tested beams. To determine the σ_n^{cr} - ε_n^{cr} that characterizes the fracture mode I propagation in the SFRSCC under the framework of a multidirectional smeared crack approach (Figure 4), an inverse analysis was executed by fitting with the minimum error the average force-deflection curve recorded in the experimental tests. The finite element mesh is represented in Figure 5, which shows that the material nonlinear analysis

was restricted to the finite elements that discretize the volume of SFRSCC ahead of the notch, whose the width is equal to the width of the notch (5 mm). The crack band width, l_b, (Figure 4), i.e., the characteristic length that bridges crack width and crack normal strain concepts, was assumed equal to the notch width (5 mm), as it was assumed that the failure crack has progressed at the notched plane, orthogonal to the axis of the beam. In order to force the cracked plane to progress along the symmetry axis of the specimen, a Gauss-Legendre integration scheme of 1×2 points was adopted. The obtained σ_n^{cr} - ε_n^{cr} diagram is represented in Figure 6, where the values that define this diagram, as well as the mode I fracture energy, G_f, derived from the area under the σ- ε_n^{cr} (where $\varepsilon_n^{cr} = w/l_b$) diagram are indicated in Table 4.

3.2.2 GFRP bars

GFRP bars are basically stressed in tension and their mechanical response can be supposed elastic up to failure. Thus, a linear elastic stress-strain relationship can be assumed for the truss elements introduced in the FE model for simulating the behaviour of GFRP bars. Table **2** includes the modulus of elasticity and the ultimate strain adopted in the FE simulations.

3.2.3 Interface finite elements to simulate the bond-slip

Interface finite elements are used to simulate the bond behaviour between GFRP bars and surrounding SFRSCC. In particular, 4-nodes-2D-interface finite elements were selected for this purpose. The sliding behaviour of such interface elements is defined by the bond-slip relationship represented in Figure 7, which is characterised by the following three branches:

$$\tau = \frac{\tau_0}{s_0} \cdot s \Rightarrow 0 \le s \le s_0 \tag{1a}$$

$$\tau = \tau_m \cdot \left(\frac{s}{s_m} \right)^{\alpha} \Rightarrow s_0 \le s \le s_m \tag{1b}$$

$$\tau = \tau_m \cdot \left(\frac{s}{s_m} \right)^{-\beta} \Rightarrow s > s_m \tag{1c}$$

where τ_0 of Eq. (1a) is obtained from Eq. (1b) by replacing s by s_0. Therefore, the main parameters required to define the sliding component of the constitutive law of the interface finite elements are: s_0 (slip at the end of the linear branch), τ_m (maximum bond stress), s_m (slip corresponding to τ_m), α and β (factor that defines the shape of the pre-peak and post-peak branch, respectively).

Theoretically α can range from 0 to infinity, but for values greater than 1 the branch described by Eq. (1b) has a τ–s convex configuration, which is not representative of the behaviour observed in experimental tests. Thus, it was assumed that α can assume values in the interval between 0 and 1. For α=1 a pre-peak linear branch is assumed, while for α=0 a constant bond stress of τ_m is considered in the interval $s_0 \le s \le s_m$. By increasing the value of β, from 0 to infinity, a more pronounced decay of bond stress transference is simulated for the post-peak phase. For β=0 it is assumed that a constant bond stress equal to the bond strength, τ_m, is assumed for $s>s_m$.

3.3 Nonlinear analyses

The above mentioned FE model was employed to simulate the behaviour observed in pull-out bending tests, namely the pull-out force versus loaded end and free end slips. All geometric and mechanical parameters needed to define concrete and bar element properties were determined from experimental programs carried out on materials employed in pull-out bending tests fully reported in [31]. On the contrary, the five parameters of the bond-slip law defined in subsection 3.2.3 were completely unknown, as they depend on the bond interaction between two innovative materials (namely, GFPR and SFRSCC) for which no well-established bond-slip relationships were available.

This study has the purpose of calibrating the interface bond-slip law for GFRP bars embedded into SFRSCC. Thus, an inverse analysis procedure was executed with the above described FE model, in order to find numerically the values of the parameters defining the bond-slip relationship (1) that conduct to the best-fit of the experimental results in terms of pull-out force and the corresponding slips (measured at either

loaded and free end). The proposed method for calibrating the interface bond-slip relationship can be regarded as an inverse identification procedure [9][37]. The above mentioned five parameters can be collected in the vector $\mathbf{q}=[s_0;s_m;\tau_m;\alpha;\beta]$ and the proposed calibration can formally be described by the following optimisation problem:

$$\bar{\mathbf{q}} = \underset{\mathbf{q}}{\operatorname{argmin}} \left\{ \sum_{i=1}^{n} \left[F_{exp,1-2}^{(i)} - F_{num}^{(i)}(s_i, \mathbf{q}) \right]^2 \right\} \tag{2}$$

where $F_{exp,1-2}$ is the average pull-out force value of each couple of identical specimens measured in the experimental program for the interface slip s_i, and $F_{num}(s_i;\mathbf{q})$ is the corresponding numerical prediction that depends on the current values of the pull-out parameters collected in $\mathbf{q}$. Slip values s_i ranging between 0 to 5 mm were actually considered and, then, n is the number of experimental measures recorded in this range. Moreover, the following error term was defined as a quantitative parameter of the matching between the experimental measures and the corresponding numerical predictions based on the identified parameters collected in the vector $\bar{\mathbf{q}}$:

$$\Delta = \frac{\sum_{i=1}^{n} \left[F_{exp,1-2}^{(i)} - F_{num}^{(i)}(s_i, \bar{\mathbf{q}}) \right]^2}{\left[F_{exp,1-2}^{(n)} \right]^2} . \tag{3}$$

Within this general framework, each nonlinear FE analysis was performed in displacement control by increasing step-by-step the relative displacement between concrete (point A_{FRC} in Figure 3) and loaded-end of GRFP bar (point A_{GFRP} in Figure 3). At the end of each analysis two curves relating pull-out force versus loaded and free ends were determined by considering the following quantities:

- The slip at the loaded end was actually assumed as the controlled displacement component;
- The slip at the free end was determined as the difference between the two horizontal absolute displacements obtained in points B_{FRC} and B_{GFRP} (Figure 3), belonging to concrete and reinforcing bar, respectively;

– The pull-out force in the GFRP in correspondence to a certain loaded and free end slip was considered as the reaction at the support S_1 (Figure 3).

The numerical simulations were interrupted at 5 mm of slip at the loaded-end, since above this slip value the experimental results showed that pull-out force decreased as slip kept growing.

4 NUMERICAL RESULTS

4.1 Calibration of the FE models

An iterative search for the "optimal" bond-slip law was carried out for each couple of identical tested specimens according to the procedure outlined in section 3.3. This section proposes the comparisons between experimental results [31] and numerical simulations in terms of force versus loaded and free end slip relationships ($F\text{-}s_l$; $F\text{-}s_f$) obtained by adopting the above mentioned "optimal" bond-slip laws.

Figure 8 reports the $F\text{-}s_l$ and $F\text{-}s_f$ comparisons obtained for specimens with 8-mm deformed bars, from which it is evident that the numerical procedure is capable of fitting with high accuracy the experimental responses. Each diagram shows the relevant experimental-to-numerical comparison by considering the three different cases of bond length investigated in experimental tests and outlined below:

- Five times the nominal bar diameter (denoted as "5Φ" in the following graphs);
- Ten times the nominal bar diameter (denoted as "10Φ" in the following graphs);
- Twenty times the nominal bar diameter (denoted as "20Φ" in the following graphs).

The only exception to the general trend of good prediction has occurred in the test nº 12 (i.e., 20Φ of bonding length and 30 mm of concrete cover, Figure 8d), which can be justified by the premature tensile failure of the GFRP bar registered experimentally [31]. Table 5 reports the numerical values of the relevant parameters that identify the bond-slip laws subjacent to the numerical simulations represented in Figure 8.

The final experimental-to-numerical comparisons obtained for specimens with bars of 12 mm nominal diameter (either smooth or deformed) confirm the high accuracy of the FE simulations performed by assuming the calibrated bond-laws. Thus, figures showing such comparisons are omitted herein for the sake of brevity, but as indicated by the error values in Tables 5 to 7, the predictive performance was similar in all the tested series.

4.2 Results of the numerical calibrations

The Eq. (1) that defines the bond-slip law is defined by the following five parameters: two slips (i.e., "s_0" and "s_m"), one interface shear stress (i.e., "τ_m") and two shape-function coefficients (i.e., "α" and "β").

This section focuses on analysing the values obtained by calibrating the above mentioned parameters for the various tested specimens. It aims at pointing out the possible influence of geometric and mechanical properties (i.e., surface treatment, concrete cover, bar diameter and bonding length) on the bond-slip law.

4.2.1 Results in terms of s_0

The parameter s_0 represents the slip corresponding to the end of linear phase of local bond relationship. The linear range is only a small part of all the pull-out force-slip relationship. As a matter of fact, Table 5, 6 and Table 7 point out that the values s_0 are almost unaffected by the variable properties considered in this study (i.e., bonding length, concrete cover, surface treatment and bar diameter). A constant value s_0=0.03 mm can be assumed in all cases.

4.2.2 Results in terms of τ_m

The parameter τ_m represents the maximum interface shear of the bond relationship. It is of key importance in influencing the actual bond behaviour of GFRP bars. The FE calibrations demonstrated that it is affected by all relevant geometric properties considered in the present study (see Tables 5 to 7):

- the τ_m has decreased with the increase of the bond length. This decrease was more pronounced from "5Φ" to "10Φ" than from "10Φ" to "20Φ";
- the concrete cover thickness plays a positive role on the values of τ_m, as higher values of bond stress were obtained for the thicker concrete cover; it is worth noting that concrete splitting cracks were observed in tests with 12-mm deformed bars with 15-mm concrete cover [31], and the numerical calibration of the bond-slip law actually led to the lowest values of τ_m in such cases;
- as expected, the surface treatment has an influence on the maximum bond stress τ_m, whose values were significantly higher (about 10%) for deformed bars.

The stress field transferred from the bar to the surrounding SFRSCC increases with the bond length. Since the material nonlinear behaviour due to crack initiation and propagation of the surrounding SFRSCC was simulated in the analyses

carried out, the level of damage introduced into the SFRSCC increases with the bond length. In consequence, the confinement provided of SFRSCC to the GFRP bar, as well as the sliding resisting mechanisms decrease with the bond length, leading to a decrease in the bond strength and a decrease of the slip at peak bond stress.

4.2.3 Results in terms of s_m

The s_m is the slip corresponding to the maximum interface shear stress (τ_m). This parameter influences significantly the bond-slip relationship, as it defines the limit between the hardening and the softening phases of the bond-slip law considered in the present study (Figure 7).

Table 5, 6 and Table 7 highlight that s_m is affected by bond length, bar diameter, concrete cover and surface treatment. In particular, the value of s_m is higher for:

- bars with longer bond length;
- bars with larger concrete cover thickness;
- deformed bars than for smooth bars.

4.2.4 Results in terms of α

The α exponent defines the trend of bond-slip relationship in the ascending branch of the curve from the end of linear phase up to the peak bond strength. Based on the results of the identification procedure carried out through the presented FE model, the bond behaviour observed in experimental tests under consideration is almost unaffected by this parameters and a constant value α=0.15 can be assumed in all case, regardless the bond length, concrete cover, diameter and surface treatment of bars.

4.2.5 Results in terms of β

The β parameter defines the shape of bond-slip relationship in the softening range. Table 5, 6 and Table 7 report the values of β obtained from the numerical simulations, and highlight that this parameter is mainly affected by the variation of the concrete cover-to-diameter ratio in the case of deformed bars. In fact, in this case, β ranges from 0.15 to 0.30 when the concrete cover-to-diameter ratio ranges from 1.14 (i.e., bar

diameter of 13.1 mm and cover thickness of 15 mm) to 3.49 (i.e., bar diameter of 8.6 mm and cover thickness of 30 mm). For smooth bars a constant value of 0.34 can be assumed for parameter β, especially for longer bond length (i.e., 10Φ and 20Φ).

4.3 Proposed correlations between bond-slip law and the specimens properties

Based on the behavioural observations remarked in the previous subsections, possible quantitative correlations between the calibrated values for the above mentioned bond parameters (i.e., τ_m, s_m, and β) and the key geometric and mechanical properties of the various specimens (i.e., bond length, bar diameter, surface treatment and concrete cover) are proposed in this section.

Firstly, the trend of τ_m versus bond length-to-diameter ratio (L_b/d) reported in Figure 9 for the values of C/d parameters considered in the present experimental program (C is the concrete cover and d is the bar diameter) suggests that τ_m can be obtained from the following Eq.:

$$\tau_m = \tau_0 \cdot \left(\frac{C}{d}\right)^{\gamma_1} \cdot \left(\frac{L}{d}\right)^{\gamma_2} \tag{4}$$

where τ_0 can be expressed as function of the concrete compressive strength ($\tau_0 = (f_{cm})^{\gamma_3}$). A mathematical power function (i.e. $y = ax^b$) was fitted to the experimental results, taking into account the two groups of concrete cover (15 and 30 mm). The results of this fitting analysis are reported in Table 8 and the related curves are plotted in Figure 9. The empirical values for γ_1, γ_2 and γ_3 may be 0.264 (the mean value), 0.340 and 0.778, respectively, for the types of GFRP and SFRSCC utilized in this study.

The numerical results for s_m show a rather irregular variation, and no simple correlations can be found for this parameter. Although this, some reasonable values can be proposed for defining s_m that is mainly affected by the bond length-to-diameter ratio:

- s_m ranging from 0.25-0.35 mm in the case of 5Φ bond length;
- s_m ranging from 0.40-1.00 mm in the case of 10Φ bond length;
- s_m ranging from 0.50-1.10 mm in the case of 20Φ bond length.

5 CONCLUSIONS

The numerical results and the inherent discussion presented in the present paper are intended to contribute for defining a bond stress-slip relationship (τ-s) capable of simulating the bond behaviour of glass fibre reinforced polymer (GFRP) bars embedded into steel fibre reinforced self-compacting concrete (SFRSCC). The values of the parameters that define the τ-s equation were obtained from an inverse identification procedure based on minimising the difference between the experimental results and the final numerical simulation. Possible correlations between the values of such parameters and the key geometric properties of the tested specimens were, then, recognised. In this regard, the following remarks can be underlined:

- under the qualitative standpoint, stable relationships were figured out between two of such relevant parameters (namely, the maximum bond stress τ_m, the corresponding slip s_m and the β exponent which control the softening branch) and the key geometric properties of tested specimens, whereas the two remaining ones (i.e, s_0 and α) were almost invariant for the various specimens;
- under the quantitative stand point, the cover-to-diameter C/d ratio was recognised as the one that more affects the shape of the bond-slip law. In fact the C/d ratio controls the possible occurrence of splitting throughout the concrete cover, which has a detrimental effect on the bond of GFRP bars embedded into concrete;
- as expected, the surface treatment of the GFRP bars had a key role in affecting the bond behaviour of bars, even though the influence could even be higher than observed, if no splitting phenomena has occurred in the case of low C/d values and deformed bars;
- possible analytical correlations (or constant value) were derived for expressing the relevant parameters of the bond-slip curve as a function of the key geometric properties; such correlations could be useful to simulate the behaviour of GFRP bars embedded in SFRSCC, depending on the actual values of geometric properties of the specimen under consideration (i.e., bar diameter, concrete cover, surface treatment, acc.).

Moreover, the inverse identification procedure employed to determine the bond-slip laws for a series of specimens tested in pull-out bending confirmed the high predictive performance of FEMIX V4.0. In these nonlinear material FEM-based simulations the bond behaviour was simulated through zero-thickness finite interface elements.

Finally, the results presented in this paper to describe the bond behaviour of GFRP bars embedded into SFRSCC can be employed for global analysis of structural members made of such materials.

ACKNOWLEDGEMENTS

The study presented in this paper is part of the research project titled “DURCOST - Innovation in reinforcing systems for sustainable pre-fabricated structures of higher durability and enhanced structural performance” with reference number of PTDC/ECM/105700/2008. The authors also thank the collaboration of the following companies: Sireg and Schoeck for providing the GFRP bars, Casais to manufacture the moulds, Maccaferri for supplying the steel fibres, Secil/Unibetão for providing the Cement, SIKA for supplying the superplasticizers; CiviTest for the production of SFRSCC specimens. Finally, the financial support provided by the EU-funded Erasmus Life-Long Programme to cover the mobility of Mr. Marco Pepe from the University of Salerno to the University of Minho for his Master Project is gratefully acknowledge.

6 REFERENCES

[1]. CEB-FIB. Model Code for Service Life Design. Bulletin 34. Task Group 5.6.

[2]. Al-Amoudi OSB, Al-Kutti WA, Ahmad S, Maslehuddin M. Correlation between Strength and certain Durability Indices of Plain and Blended Cement Concretes. Cement Concrete Comp 2009; 31(9):672-76.

[3]. Abosrra L, Ashour AF, Youseffi M. Corrosion of steel reinforcement in concrete of different compressive strengths. Constr Build Mater 2011; 25(10):3915-25.

[4]. Steffens A; Dinkler D; Ahrens H. Modeling carbonation for corrosion risk prediction of concrete structures. Cement Concrete Res 2002; 32(6):935-41.

[5]. Ryu DW, Ko JW, Noguchi T. Effects of simulated environmental conditions on the internal relative humidity and relative moisture content distribution of exposed concrete. Cement Concrete Comp 2001; 33(1):142-53.

[6]. Saadatmanesh H, Ehsani MR. Fiber Composite Bar for Reinforced Concrete Construction. J Compos Mater 1991; 25(2):188-203.

[7]. CEB-FIB. FRP reinforcement in RC structures. Bulletin No. 40. Ghent; 2007.

[8]. ACI Committee 440. Guide for the Design and Construction of Structural Concrete Reinforced with FRP Bars (ACI 440.1R-06). Farmington Hills (MI): American Concrete Institute; 2006.

[9]. Italian National Council of Research. Guide for the Design and Construction of Concrete Structures Reinforced with Fiber-Reinforced Polymer Bars. CNR – DT203/2006; 2006. (available online at http://www.cnr.it/documenti/norme/IstruzioniCNR_DT203_2006_eng.pdf, accessed on August 1st 2012);

[10]. Micelli F, Nanni A. Durability of FRP rods for concrete structures. . Constr Build Mater 2004; 18(7):491-503.

[11]. Faza SS, GangaRao HVS. "*Glass FRP reinforcing bars for concrete*", Fiber-reinforced-plastic (FRP) reinforcement for concrete structures; properties and applications; Developments in Civil Engineering; 42, A. Nanni, ed., Elsevier Science Publishers.

[12]. Kocaoza S, Samaranayakeb VA, Nanni A. Tensile characterization of glass FRP bars. Compos Part B-Eng 2005; 36(2):127-34.

[13]. Achillides Z, Pilakoutas K. Bond Behavior of Fiber Reinforced Polymer Bars under Direct Pullout Conditions. J Compos Construct ASCE 2004; 8(2):173-81.

[14]. Caggiano A, Martinelli E. A unified formulation for simulating the bond behaviour of fibres in cementitious materials. Mater Design 2012; 42:204–13;

[15]. CEB-FIB, Bond of reinforcement in concrete, State-of-art Report. Bulletin 10. fib-International Federation for Concrete : Switzerland, Lausanne; 2000.

[16]. CNR DT 203. Guide for the Design and Construction of Concrete Structures Reinforced with Fiber-Reinforced Polymer Bars. 2006.

[17]. CEB-FIB. Model Code 2010 First complete draft Volume 1. Bulletin 55. fib-International Federation for Concrete: Switzerland, Lausanne; 2010.

[18]. Daniali S. Development length for fiber-reinforced bars. Proceeding of 1st International Conference on Advanced Composite Materials in Bridges and Structures CSCE. :1992. p. 179-88.

[19]. Tepfers R, Molander I, Thalenius K. Experience from testing of concrete reinforced with carbon fiber and aramid fiber strands. XIV. Nordic Concrete Congress & Nordic Concrete Industry Meeting, Icelandic Concrete Association, Reykjavik 1992.p. 337-47.

[20]. Malvar LJ. "*Bond stress–slip characteristics of FRP rebars*", Technical Report TR-2013-SHR, Naval Facilities Engineering Service Center 1994. Port Hueneme, California, CA 93043-4328, 45.

[21]. Malvar, LJ. Tensile and Bond Properties of GFRP Reinforcing Bars. ACI Mater J 1995; 92(3):276-85.

[22]. Eligehausen R, Popov E, Bertero VV. Local Bond Stress-Slip Relationships of Deformed Bars under Generalized Excitations. Report N° 83/23, EERC, University of California at Berkeley: 162; 1983.

[23]. Cosenza E, Manfredi G, Realfonzo R. Analytical modelling of bond between FRP reinforcing bars and concrete. In: Non Metallic (FRP) Reinforcement for Concrete Structures (L. Taerwe ed.), E&FN SPON, 1995.

[24]. Alunno Rossetti V, Galeota D, Gianmatteo MM. Local bond stress-slip relationships of glass fibre reinforced plastic bars embedded in concrete. Mater Struct 1995; 28(6): 40-44.

[25]. Tepfers R, De Lorenzis L. Bond of FRP reinforcement in concrete - a challenge. Mech Compos Mater 2003; 39(4):315-28.

[26]. Malvar LJ, Cox JV, Cochran KB. Bond between carbon fiber reinforced polymer bars and concrete. I: Experimental study. J Comp Construct ASCE 2003; 7(2):154–63.

[27]. Sena-Cruz JM, Barros JAO. Bond Between Near-Surface Mounted Carbon-Fiber-Reinforced Polymer Laminate Strips and Concrete. J Compos Construct ASCE 2004; 8(6):519-27.

[28]. Bianco V, Barros JAO, Monti G. Bond model of NSM-CFRP in the context of the shear strengthening of RC beams. J Struct Eng ASCE 2009; 135(6), 619-631;

[29]. Okelo R, AM ASCE, Yuan RL, PE. Bond Strength of Fiber Reinforced Polymer Rebars in Normal Strength Concrete. J Compos Construct ASCE 2005; 9(3): 203-13.

[30]. Tighiouart B, Benmokrane U, Gao D. Investigation of bond in concrete member with fibre reinforced polymer (FRP) bars. Const Build Mater 1998; 12(8):453-62.

[31]. Mazaheripour H, Barros J, Sen-Cruz J, Pepe M, Martinelli E. Experimental study on bond performance of GFRP bars in self-compacting steel fiber reinforced concrete. Compos Struct 2012; 95:202-12.

[32]. Sena-Cruz J, Barros JAO, Azevedo A, Ventura Gouveia A. Numerical simulation of the nonlinear behavior of RC beams strengthened with NSM CFRP strips. CMNE 2007 - Congress on Numerical Methods in Engineering e XXVIII CILAMCE - Iberian Latin American Congress on Computational Methods in Engineering, Article no. 485, FEUP, Porto 2007.

[33]. RILEM/CEB/FIP. Test of the bond strength of reinforcement of concrete: test by bending, Recommendation RC.5, 5; 1978.

[34]. Sena-Cruz JM. Strengthening of concrete structure with near-surface mounted CFRP laminate strips. Ph.D. thesis: Civil Engineering Department of University of Minho; 2004.

[35]. CEB-FIP. Model Code 2010 (final draft). Switzerland, Lausanne; 2011.

[36]. Faella C, Martinelli E, Nigro E. Direct Versus Indirect Method For Identifying FRP-to-Concrete Interface Relationships. J Compos Construct ASCE 2009; 13(3): 226-33.

[37]. Martinelli E, Napoli A, Nunziata B, Realfonzo R. Inverse identification of a bearing-stress-interface-slip relationship in mechanically fastened FRP laminates. Compos Struct 2012; 94(8):2548-60.

Figure 1: GFRP bars employed in the experimental program [31]

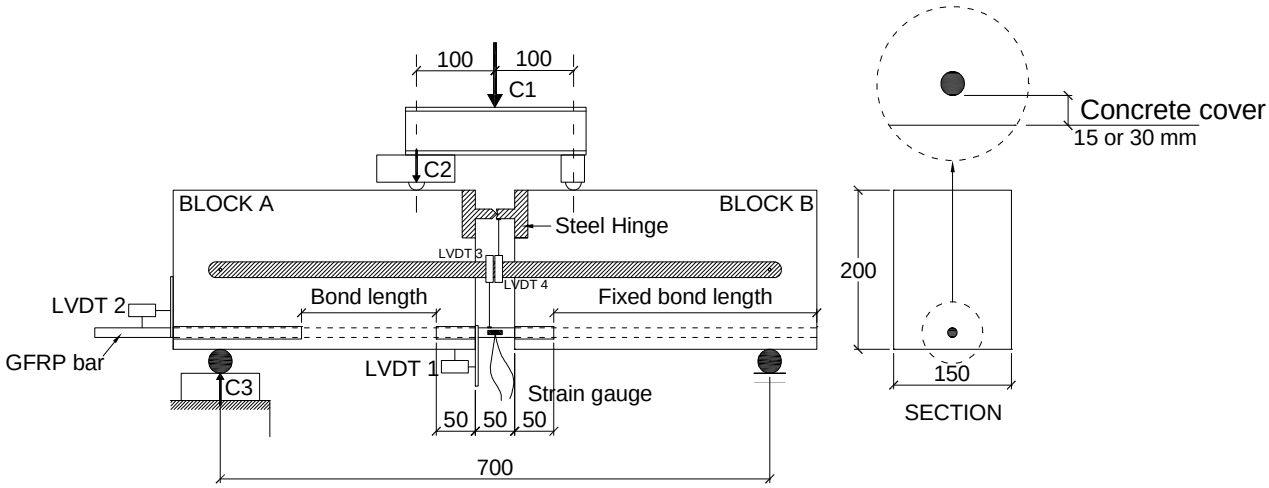

Figure 2: Pull-out-bending test setup

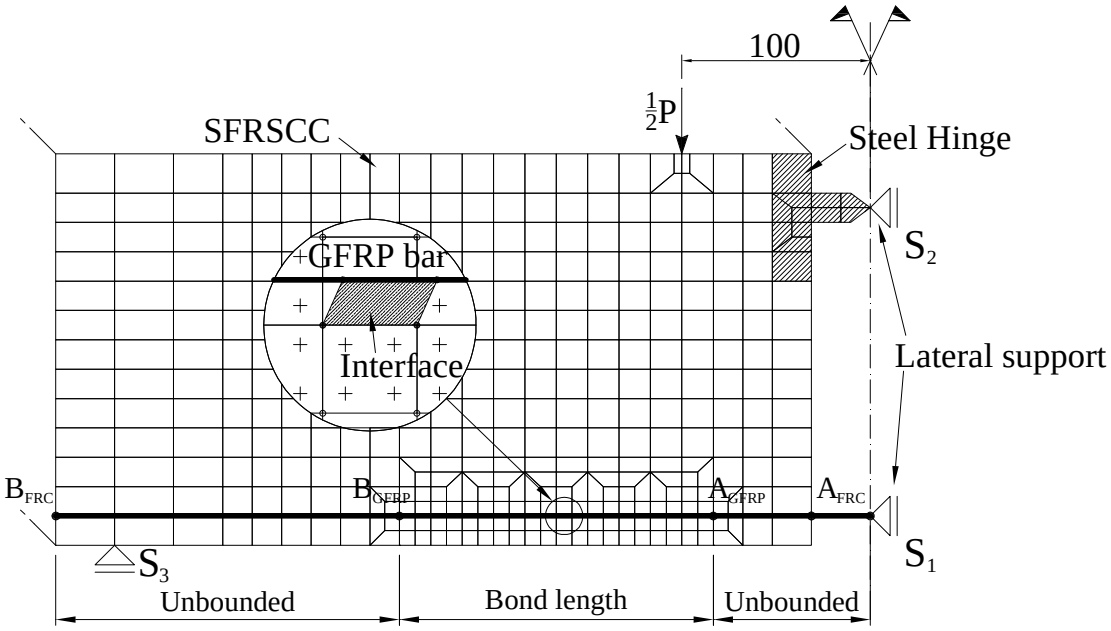

Figure 3: FE Model

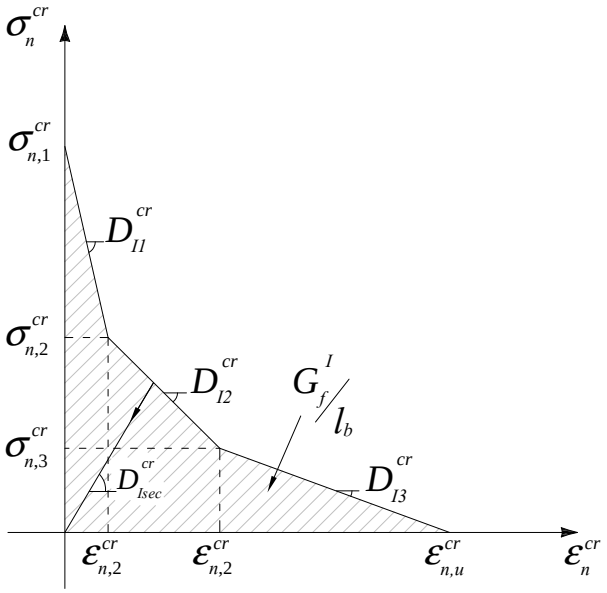

Figure 4: Trilinear stress-strain diagram to simulate the fracture mode I crack propagation ($\sigma_{n,2}^{cr} = \alpha_1 \, \sigma_{n,1}^{cr}$, $\sigma_{n,3}^{cr} = \alpha_2 \, \sigma_{n,1}^{cr}$, $\varepsilon_{n,2}^{cr} = \xi_1 \, \varepsilon_{n,u}^{cr}$, $\varepsilon_{n,3}^{cr} = \xi_2 \, \varepsilon_{n,u}^{cr}$).

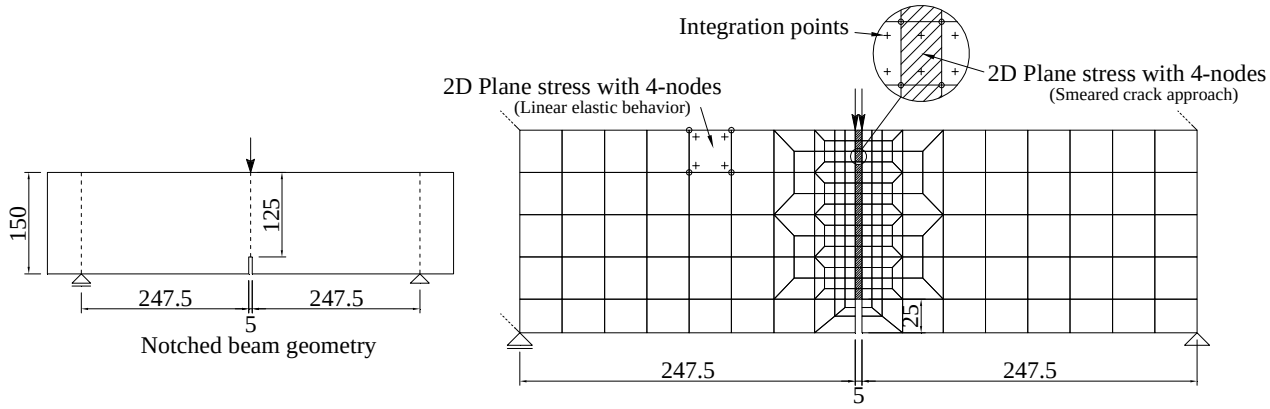

Figure 5: FEMIX model to simulate the notched beam bending tests on SFRSCC (dimensions in mm)

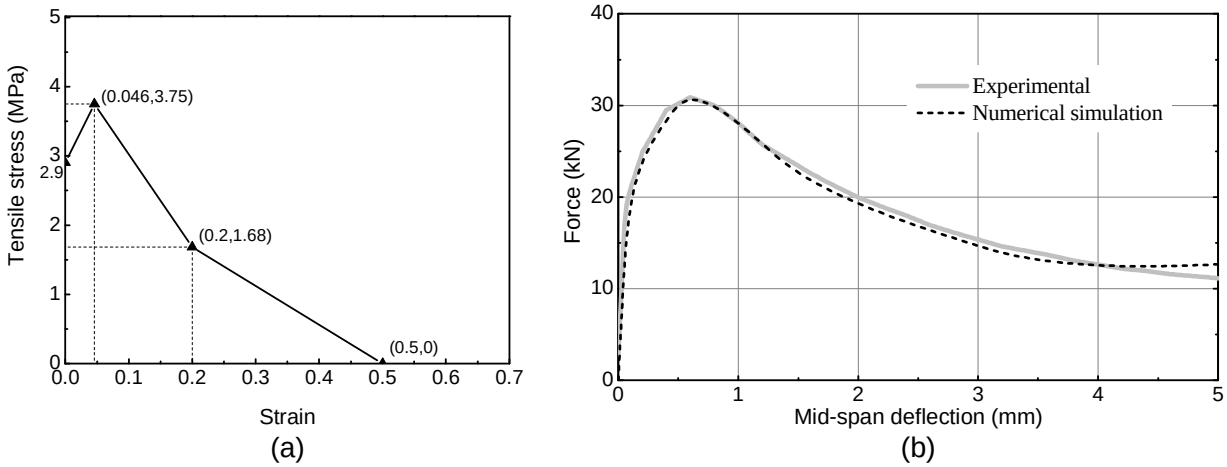

Figure 6: Tensile stress versus crack width and strain diagram (a) derived from inverse analysis (b)

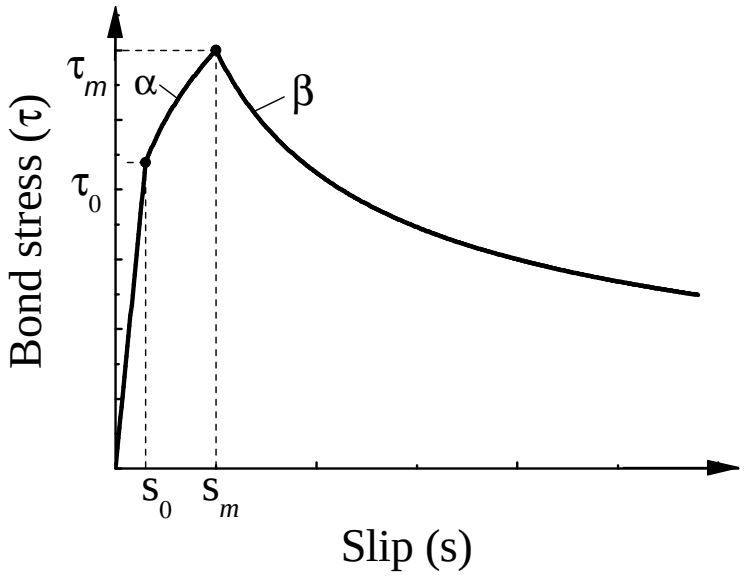

Figure 7: General bond-slip law

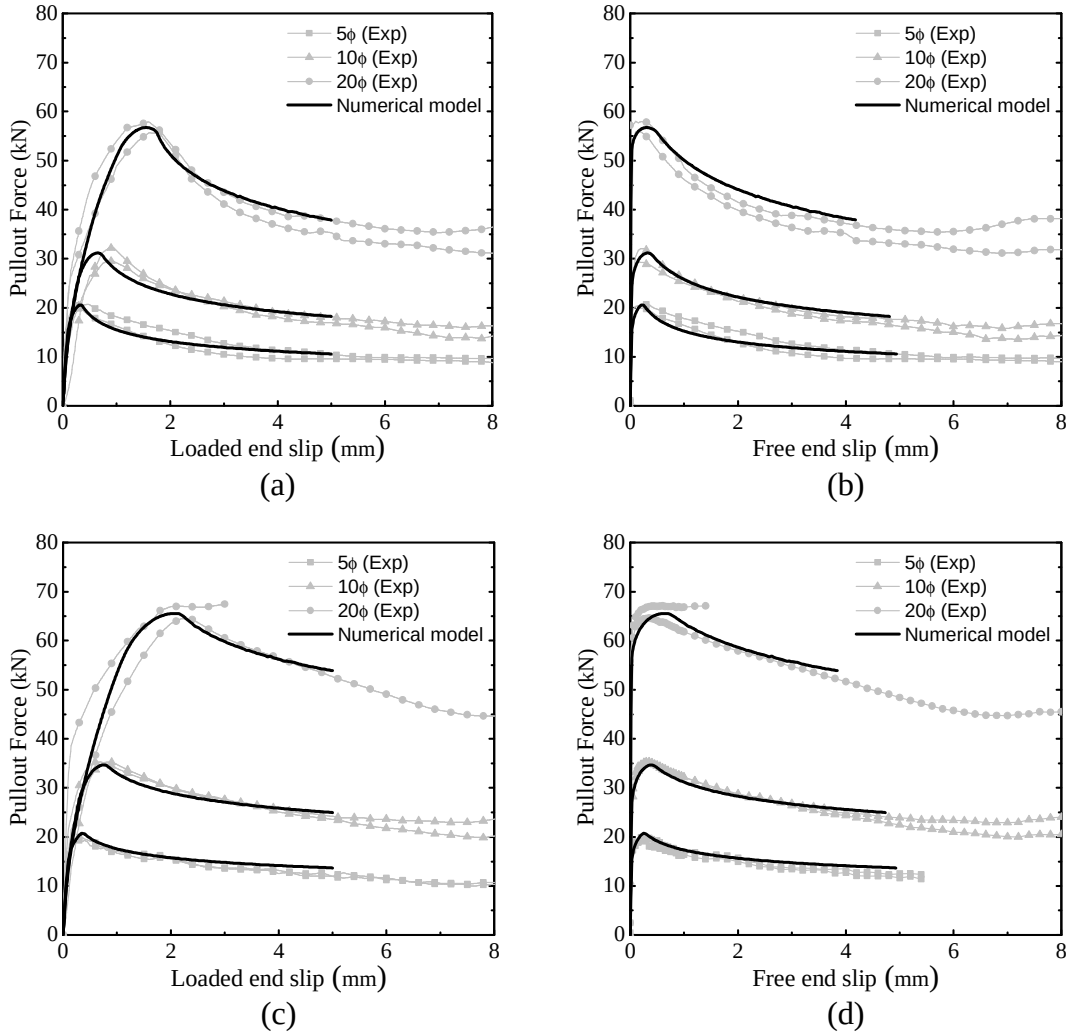

Figure **8**: Numerical-experimental comparisons for 8 mm deformed bars: (a), (b) concrete cover 15 mm; (c), (d) concrete cover 30 mm

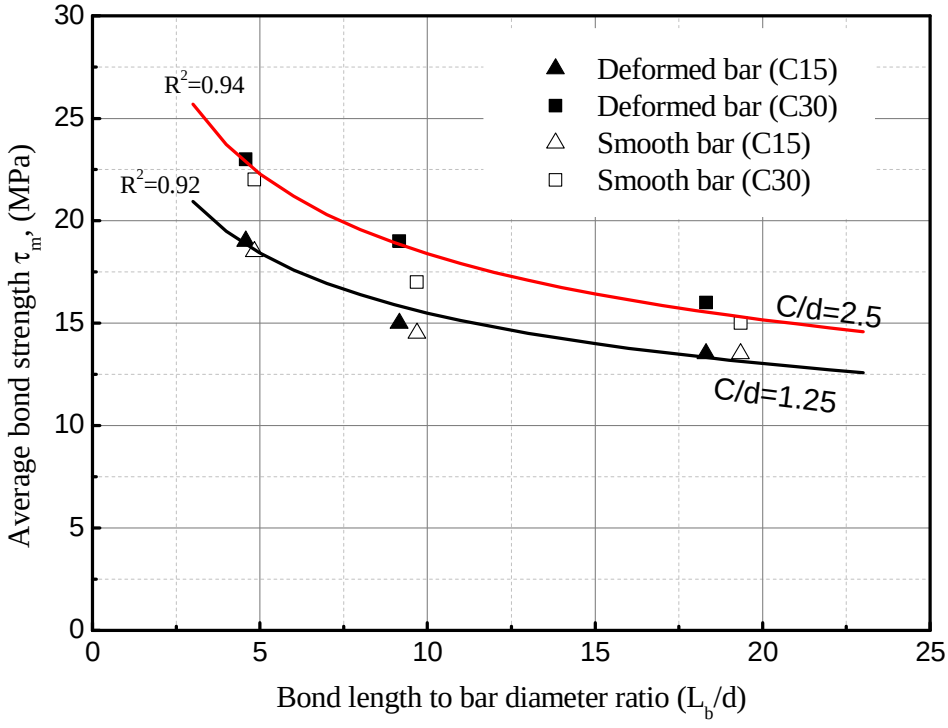

Figure **9**: Correlation between τ_m and length-to-diameter ratio with considering concrete cover effect

Table 1: Basic mechanical properties of SFRSCC

Compressive strength f_c	*Young modulus* E_c	*Flexural tensile strength*(1) f_{fct}
MPa	*GPa*	*MPa*
63.7	30.4	2.9

() – Obtained according to [17]

Table 2: Geometric and mechanical properties of GFRP bars

Nominal Diameter mm	*Measured Diameter mm*	*Producer*[*]	*Type of surface*	*Elastic modulus*[**] *MPa*	*Tensile strength*[**] *MPa*	ε_u[**]
8	8.6	A	Deformed with rib and groves	64000	~1000	7.4 %
12	13.1	A	Deformed with rib and groves	55000	~1000	7.4 %
12	12.4	B	Sand-coated	49000	~1000	4.4 %

* Fictitious denomination of the companies that supplied the GFRP bars; [**]Values provided by the supplier;

Table 3: Experimental tests

Surface treatment	*Bar diameter (Φ) mm*	*Concrete cover mm*	*Bond length*	*Specimen n°*
Deformed	8.6	15	5 Φ	01-02
			10 Φ	05-06
			20 Φ	09-10
		30	5 Φ	03-04
			10 Φ	07-08
			20 Φ	11-12
Deformed	13.1	15	5 Φ	13-14
			10 Φ	17-18
			20 Φ	21-22
		30	5 Φ	15-16
			10 Φ	19-20
			20 Φ	23-24
Smooth	12.4	15	5 Φ	25-26
			10 Φ	29-30
			20 Φ	33-34
		30	5 Φ	27-28
			10 Φ	31-32
			20 Φ	35-36

Table 4: Values of the mechanical parameters adopted for simulating the behaviour of SFRSCC in tension

Parameter	*Value*
Compressive strength	63.7 MPa
Tensile strength	2.9 MPa
ξ_1	0.09
α_1	1.293
ξ_2	0.393
α_2	0.579
G_f	4.187 N/mm

Table 5: Numerical results for 8 mm deformed bars

Specimen configuration					Adopted bond slip law					
Specimen n°	*Surface treatment*	*Bar diameter mm*	*Concrete cover mm*	*Bond length*	s_0 *mm*	s_m *mm*	τ_m *MPa*	α	β	*error %*
01-02	Deformed	8.6	15	5 Φ	0.03	0.25	19.5	0.15	0.23	0.4
05-06				10 Φ	0.03	0.40	15.0	0.15	0.23	1.8
09-10				20 Φ	0.03	0.50	13.5	0.15	0.23	0.6
03-04			30	5 Φ	0.03	0.28	19.5	0.15	0.15	0.4
07-08				10 Φ	0.03	0.45	16.5	0.15	0.15	0.1
11-12				20 Φ	0.03	0.80	16.0	0.15	0.15	0.5

Table 6: Numerical results for 12 mm deformed bars

Specimen configuration					Adopted bond slip law					
Specimen n°	*Surface treatment*	*Bar diameter mm*	*Concrete cover mm*	*Bond length*	s_0 *mm*	s_m *mm*	τ_m *MPa*	α	β	*error %*
13-14	Deformed	13.1	15	5 Φ	0.03	0.26	19.0	0.15	0.30	0.2
17-18				10 Φ	0.03	0.50	15.0	0.15	0.30	0.5
21-22				20 Φ	0.03	0.80	13.5	0.15	0.30	0.5
15-16			30	5 Φ	0.03	0.28	23.0	0.15	0.18	0.3
19-20				10 Φ	0.03	1.00	19.0	0.15	0.20	1.6
23-24				20 Φ	0.03	1.10	16.0	0.15	0.20	0.5

Table 7: Numerical results for 12 mm smooth bars

Specimen configuration					Adopted bond slip law					
Specimen n°	*Surface treatment*	*Bar diameter mm*	*Concrete cover mm*	*Bond length*	s_0 *mm*	s_m *mm*	τ_m *MPa*	α	β	*error %*
25-26	Smooth	12.4	15	5 Φ	0.03	0.35	18.5	0.15	0.28	0.9
29-30				10 Φ	0.03	0.40	14.5	0.15	0.34	0.3
33-34				20 Φ	0.03	0.40	13.5	0.15	0.34	2.7
27-28			30	5 Φ	0.03	0.35	22.0	0.15	0.22	1.1
31-32				10 Φ	0.03	0.90	17.0	0.15	0.34	0.9
35-36				20 Φ	0.03	0.90	15.0	0.15	0.34	0.8

Table 8: The results of fitted curves in terms of the maximum bond shear stress versus the *L/d* ratio

Analysis number	*C/d*	*a*	*b*	R^2	γ_1	γ_2	γ_3
1	2.5	34.38	-0.278	0.939	-0.278	0.340	0.778
2	1.25	27.14	-0.250	0.924	-0.250	0.340	0.778